Structural Engineering and Mechanics, Vol. 9, No. 6 (2000) 541-555
DOI: http://dx.doi.org/10.12989/sem.2000.9.6.541

Compression strength of pultruded equal leg angle sections

D. Polyzois† and I.G. Raftoyiannis‡

Department of Civil & Geological Engineering, University of Manitoba, Winnipeg, Canada

Abstract. Pultruded cross-sections are always thin-walled due to constraints in the manufacturing process. Thus, the buckling strength determines the overall strength of the member. The elastic buckling of pultruded angle sections subjected to direct compression is studied. The lateral-torsional buckling, very likely to appear in thin-walled cross-sections, is investigated. Plate theory is used to allow for cross-sectional distortion. Shear effects and bending-twisting coupling are accounted for in the analysis because of their significant role. A simplified approach for determining the maximum load of equal leg angle sections under compression is presented. The analytical results obtained in this study are compared to the manufacturer's design guidelines for compression members as well as with the design specifications for steel structural members. Experimental results are obtained for various length specimens of pultruded angle sections. The results presented in this paper correspond to actual pultruded equal leg angle sections being used in civil engineering structures.

Key words: pultruded; composites; angle sections; lateral; torsional; buckling.

1. Introduction

Various pultrusion manufacturers produce on an industrial basis structural members with a variety of cross-sectional shapes and dimensions (e.g., I-sections, channels, box-type sections, tubes, etc.). These products are made from polymers (usually called resin in the uncured state and matrix in the cured state) with fiber reinforcement. Polyester, vinylester or epoxy are used as a matrix to hold together E-glass, S-glass, aramid or carbon fibers used as reinforcement. Fibers and polymer are joined through the pultrusion process to form the desired cross-section. The present study is concerned with the design and strength of pultruded equal leg angle sections under direct compression.

An angle section column under compression can buckle with various modes depending on the geometry of the cross-section, the material properties, and the boundary conditions (Eterovic *et al.* 1990). The column can buckle either locally or globally, or with a combination of local and global modes. In local buckling, changes in the geometry of the cross-section occur, but not accompanied by lateral displacement or twist. Each leg of the angle section may buckle as a plate, where instability of both legs is coupled. In the case of global buckling, the cross-section may displace laterally and twist without local changes in the geometry or it may buckle about the weak axis in an Euler-type mode. Possible interaction between local and global modes is also investigated. Only

† Professor
‡ Post-Doc Fellow

equal leg angle sections are studied herein.

A number of studies have been conducted separately on the buckling of thin-walled sections such as I-sections and angle sections made from steel as well as composite I-section beams and columns (Raftoyiannis 1994), but only a few on angle sections. In fact, the vast majority of studies are concerned with steel members (homogeneous and isotropic material). Pultruded cross-sections are thin-walled and each leg of the cross-section is treated in this study as a laminated plate. Each lamina can be specially orthotropic or generally orthotropic. The stiffness coupling terms are important, especially when bending-twisting coupling terms are present because they produce higher instability. A simplified approach is presented herein for the determination of the critical load and simple guidelines are proposed. The results presented in this study correspond to actual pultruded equal leg angle sections (see Table 1).

2. Theoretical analysis

Pultruded cross-sections are usually thin-walled due to manufacturing constraints. Angle sections are produced with various dimensions and thicknesses. A typical equal leg angle cross-section is shown in Fig. 1(a). Each leg of the angle section can be considered as a laminate plate composed of different layers. For the Fiber Reinforced Plastic (FRP) angle sections studied herein, the laminate

Table 1 Sectional properties of equal leg angle sections

Section	t (in)	b (in)	Area (in^2)	I_x (in^4)	x_0 (in)	I_z (in^4)	J (in^4)	C_w (in^6)
4 × 4 × ¼	0.250	4.00	1.938	3.039	0.968	1.225	0.042	0.056
4 × 4 × ⅜	0.375	4.00	2.859	4.359	0.951	1.774	0.141	0.188
4 × 4 × ½	0.500	4.00	3.750	5.561	0.933	2.295	0.333	0.444
6 × 6 × ⅜	0.250	6.00	2.938	10.575	1.468	4.244	0.063	0.188
6 × 6 × ¼	0.375	6.00	4.359	15.387	1.452	6.201	0.211	0.633
6 × 6 × ½	0.500	6.00	5.750	19.908	1.435	8.071	0.500	1.500

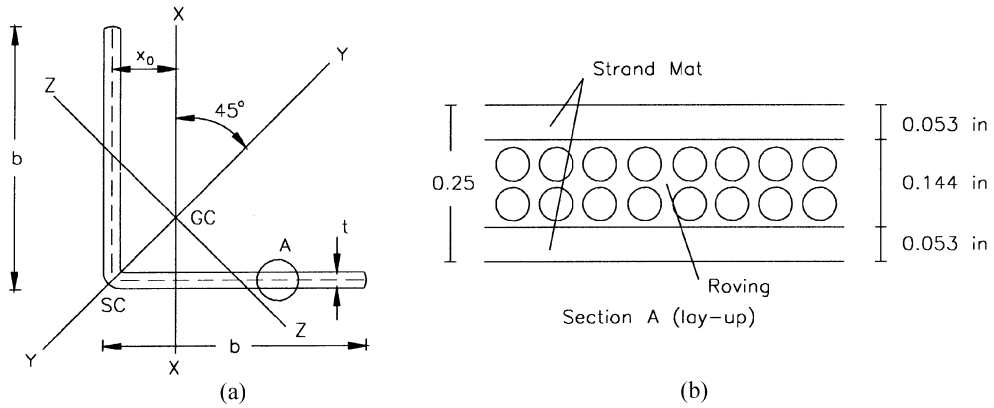

Fig. 1 (a) Geometry of a typical equal leg angle, (b) Lay-up of the ¼ in laminate

consists of two layers with fiber volume fraction 30% called roving and one layer with fiber volume fraction 50% called strand-mat. The stacking sequence as well as the layer thickness for a $4 \times 4 \times {}^{1}/_{4}$ in ($10 \times 10 \times 0.65$ cm) angle section is shown in Fig. 1(b). Using classical lamination theory, the stiffness components of an anisotropic plate can be determined. The constitutive equation for the laminate is (Gibson 1994)

$$\begin{Bmatrix} \{N\} \\ \{M\} \end{Bmatrix} = \begin{bmatrix} [A] & [B] \\ [B] & [D] \end{bmatrix} \begin{Bmatrix} \{\varepsilon\} \\ \{\kappa\} \end{Bmatrix} \tag{1}$$

where $\{N\}$, $\{M\}$, $\{\varepsilon\}$ and $\{\kappa\}$ are stress resultants, moment resultants, strains and curvatures, respectively. The stiffness coefficients A_{ij}, B_{ij} and D_{ij} ($i, j = 1, 2, 6$) correspond to membrane, membrane-bending coupling and bending actions, respectively, and are defined as follows

$$A_{ij} = \int_{-t/2}^{t/2} \overline{Q}_{ij} dz \tag{2a}$$

$$B_{ij} = \int_{-t/2}^{t/2} \overline{Q}_{ij} dz \tag{2b}$$

$$D_{ij} = \int_{-t/2}^{t/2} \overline{Q}_{ij} z^2 dz \tag{2c}$$

where t is the laminate thickness and $\overline{Q}_{ij}$ are the transformed layer stiffness components.

Taking also into account the out-of-plane shear of the laminate, the relationship between shear forces and shear strains can be written as follows:

$$\begin{Bmatrix} S_y \\ S_x \end{Bmatrix} = \begin{bmatrix} A_{44} & A_{45} \\ A_{45} & A_{55} \end{bmatrix} \begin{Bmatrix} \gamma_{yz} \\ \gamma_{zx} \end{Bmatrix} \tag{3}$$

where S_y and S_x are the out-of-plane shear resultants, and γ_j are the shear strains. The stiffness components A_{ij} ($i, j = 4, 5$) are determined using Eq. (2a) with the corresponding stiffness components $\overline{Q}_{ij}$. Note that Eqs. (1) and (3) are not coupled, i.e., membrane and/or bending deformations do not produce out-of-plane shear.

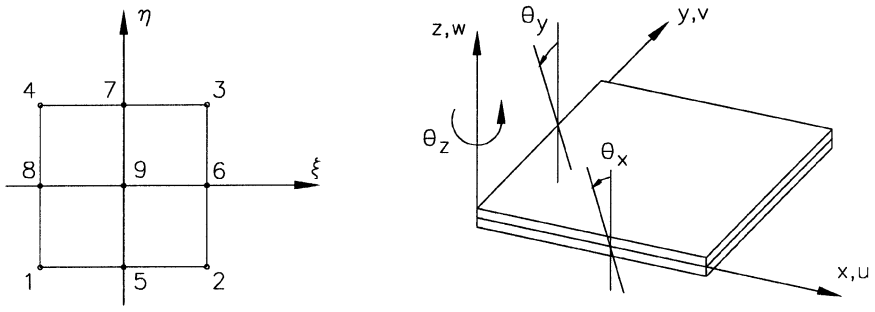

(a) (b)

Fig. 2 Composite plate element: (a) Nodes; (b) Degrees of freedom

3. Finite element analysis

A finite element program for buckling analysis of composite plates and plate assemblies (Barbero *et al*. 1993 and Barbero *et al*. 1996) is used herein to determine the critical buckling load as well as the buckling mode of FRP angle sections. The program employs a nine-node Lagrangean anisotropic plate element, see Fig. 2(a), based upon a first-order shear deformation theory. The displacement filed in this case is

$$\begin{aligned} u(x, y, z) &= u_0(x, y) - z\,\theta_x \\ v(x, y, z) &= v_0(x, y) - z\,\theta_y \\ w(x, y, z) &= w_0(x, y) \end{aligned} \tag{4}$$

where, the subscript $(\ )_0$ refers to mid-plane values, and θ_x, θ_y are the average rotations of a line initially perpendicular to the middle surface of the plate as indicated in Fig. 2(b). The displacement distributions within the element can be expressed using the nodal displacements with the aid of the shape functions N_i, as follows:

$$(u,\ v,\ w,\ \theta_x,\ \theta_y,\ \theta_z) = \sum_{i=1}^{n} N_i(u_i,\ v_i,\ w_i,\ \theta_{xi},\ \theta_{yi},\ \theta_{zi}) \tag{5}$$

A strain-displacement relation can be written for this case, where the strains $\{\varepsilon\}$ include the linear strains $\{\varepsilon_0\}$ plus the von-Karman nonlinear strains $\{\varepsilon_1\}$

$$\{\varepsilon\} = \{\varepsilon_0\} + \{\varepsilon_1\} = \begin{Bmatrix} u_{,x} \\ v_{,y} \\ u_{,y} + v_{,x} \\ -\theta_{x,x} \\ -\theta_{y,y} \\ -\theta_{x,y} - \theta_{y,x} \\ -w_{,y} - \theta_y \\ w_{,x} - \theta_x \\ \theta_z \end{Bmatrix} + \frac{1}{2} \begin{Bmatrix} w_{,x}^2 \\ w_{,y}^2 \\ 2w_{,x} + w_{,y} \\ 0 \\ 0 \\ 0 \\ 0 \\ 0 \\ 0 \end{Bmatrix} \tag{6}$$

where $(\ )_{,x}$ in Eq. (6) denotes partial differentiation with respect to variable x.

The components of the strain vector $\{\varepsilon\}$ are

$$\{\varepsilon\} = \{\varepsilon_x\ \varepsilon_y\ \gamma_{xy}\ \kappa_x\ \kappa_y\ \kappa_{xy}\ \gamma_{yz}\ \gamma_{zx}\ \theta_z\}^T \tag{7}$$

The in-plane rotation θ_z, also known as drilling degree-of-freedom, is included to account for element connectivity in the three-dimensional space and also to avoid numerical instability of the solution in the case of plate assemblies.

For the composite plate element formulated herein, the constitutive law is defined combining Eqs. (1) and (3) as follows

$$\begin{Bmatrix} N_x \\ N_y \\ N_{xy} \\ M_x \\ M_y \\ M_{xy} \\ S_y \\ S_x \\ M_z \end{Bmatrix} = \begin{bmatrix} A_{11} & A_{12} & A_{16} & B_{11} & B_{12} & B_{16} & 0 & 0 & 0 \\ A_{12} & A_{22} & A_{26} & B_{12} & B_{22} & B_{26} & 0 & 0 & 0 \\ A_{16} & A_{26} & A_{66} & B_{16} & B_{26} & B_{66} & 0 & 0 & 0 \\ B_{11} & B_{12} & B_{16} & D_{11} & D_{12} & D_{16} & 0 & 0 & 0 \\ B_{12} & B_{22} & B_{26} & D_{12} & D_{22} & D_{26} & 0 & 0 & 0 \\ B_{16} & B_{26} & B_{66} & D_{16} & D_{26} & D_{66} & 0 & 0 & 0 \\ 0 & 0 & 0 & 0 & 0 & 0 & A_{44} & A_{45} & 0 \\ 0 & 0 & 0 & 0 & 0 & 0 & A_{45} & A_{55} & 0 \\ 0 & 0 & 0 & 0 & 0 & 0 & 0 & 0 & C^* \end{bmatrix} \begin{Bmatrix} \varepsilon_x \\ \varepsilon_y \\ \gamma_{xy} \\ \kappa_x \\ \kappa_y \\ \kappa_{xy} \\ \gamma_{yz} \\ \gamma_{zx} \\ \theta_z \end{Bmatrix} \tag{8}$$

where, the stiffness properties A_{ij}, B_{ij} and D_{ij} are defined in Eqs. (2), and C^* is a very small number compared to the stiffness values and corresponds to the in-plane rotation θ_z.

The total potential energy U of the plate assembly subjected to membrane and transverse loading can now be written as

$$U=\frac{1}{2}\int_V \{\sigma\}^T\{\varepsilon\}dV-\lambda\{\delta\}^T\{f\} \tag{9}$$

where $\{\delta\}$ is the nodal displacement vector, and $\{f\}$ is the load vector scaled by a single factor λ. The stress vector $\{\sigma\}$ is in this case

$$\{\sigma\}=\{N_x \;\; N_y \;\; N_{xy} \;\; M_x \;\; M_y \;\; M_{xy} \;\; S_y \;\; S_x \;\; M_z\}^T \tag{10}$$

Buckling occurs when the second derivative of the total potential energy with respect to the nodal displacements is zero, that is

$$\frac{\partial^2 U}{\partial \delta_i^2}=\det([K]-\lambda[K_\sigma])=0 \tag{11}$$

where, $[K]$ is the stiffness matrix and $[K_\sigma]$ is the load-geometry matrix of the structure.

The angle column is discretized into 384 elements, a mesh that provides an almost exact solution. The stiffness coefficients for the laminate with thickness t=0.25 in (0.65 cm) used in this study are listed in Table 2. Note that for the angle section laminate, no shear or membrane-bending coupling

Table 2 Stiffness coefficients for the 4 × 4 × ¼ angle specimens

A_{11}	A_{22}	A_{12}	A_{66}	A_{16}	A_{26}
625000	382500	121635	106250	0	0
B_{11}	B_{22}	B_{12}	B_{66}	B_{16}	B_{26}
0	0	0	0	0	0
D_{11}	D_{22}	D_{12}	D_{66}	D_{16}	D_{26}
3255.2	1992.2	633.5	553.4	0	0
A_{44}	A_{55}	A_{45}	*) Stiffness are expressed in lbs and in		
88540	88540	0			

Table 3 Critical loads (lbs) for the angle columns by FE analysis*

L (in)	$4\times4\times1/4$	$4\times4\times3/8$	$4\times4\times1/2$	$6\times6\times1/4$	$6\times6\times3/8$	$6\times6\times1/2$
24	5339	17956	42322	5354	18070	42824
30	4597	15428	36260	4198	14162	33535
36	4194	14044	32897	3575	12529	28518
42	3949	13191	30781	3201	10785	25502
48	3787	12616	29311	2958	9964	23539
60	3599	11881	27283	2674	8994	21209
72	3471	11376	25754	2519	8460	19907

*Lateral-torsional mode observed in all cases

takes place because the laminate is symmetric with respect to the middle surface. The angle column is simply supported at both ends. A unit load vector $\{f\}$ is applied to the one end of the column and the load factor λ is computed through buckling analysis. The critical buckling loads for various lengths of commercially available equal leg angle sections are listed in Table 3.

4. Column approach

Consider a composite angle column of length L and cross-sectional area A that is subjected to a compressive load P. The geometric characteristics of the cross-section are shown in Fig. 1a. The governing equations for combined lateral-torsional instability are (Brush and Almroth 1975)

$$EI_{yy}\frac{\partial^4 w}{\partial x^4}+P\frac{\partial^2(w-y_0\phi)}{\partial x^2}=0 \tag{12}$$

$$EI_{zz}\frac{\partial^4 v}{\partial x^4}+P\frac{\partial^2(v-z_0\phi)}{\partial x^2}=0 \tag{13}$$

$$EC_w\frac{\partial^4\phi}{\partial x^4}-\left(GJ-\frac{I_0}{A}P\right)\frac{\partial^2\phi}{\partial x^2}-Py_0\frac{\partial^2 w}{\partial x^2}+Pz_0\frac{\partial^2 v}{\partial x^2}=0 \tag{14}$$

where, ϕ is the angle of rotation, E is the engineering modulus, corresponding to the longitudinal direction x, G is the in-plane shear modulus, J is the torsion constant, and I_{yy}, I_{zz} are the moments of inertia about y and z axes, respectively. The E modulus and G modulus can be determined by inverting the $[A\ B\ B\ D]$ matrix of Eq. (1) and setting $E=1/a_{11}t$, and $G=1/a_{66}\ t$. The coordinates y_0 and z_0 define the position of the shear center (see Fig. 1a) and $I_0=I_{yy}+I_{zz}+A(y_0^2+z_0^2)$. The warping constant C_w for an equal angle thin-walled section can be determined from

$$C_w=\frac{1}{18}b^3t^3 \tag{15}$$

For the case of simply supported boundary conditions, it is convenient to assume a displacement field of the following form

$$w=A_1\sin\frac{\pi x}{L} \qquad v=A_2\sin\frac{\pi x}{L} \qquad \phi=A_3\sin\frac{\pi x}{L} \tag{16}$$

Substitution of Eqs. (16) into Eqs. (12)-(14) result in a linear system of equations with respect to the coefficients A_1, A_2 and A_3. Combined instability corresponds to a non-trivial solution of the system, thus

$$\frac{I_0}{A}(P-P_\phi)(P-P_y)(P-P_z)-P^2z_0^2(P-P_y)-P^2y_0^2(P-P_z)=0 \tag{17}$$

where the loads P_ϕ, P_y and P_z correspond to pure torsional or flexural instability.

$$P_\phi=\frac{A}{I_0}\left(\frac{\pi^2EC_w}{(kL)^2}+GJ\right) \qquad P_y=\frac{\pi^2EI_y}{(kL)^2} \qquad P_z=\frac{\pi^2EI_z}{(kL)^2} \tag{18}$$

For the cross-section under study with one axis of symmetry, z_0=0, Eq. (17) simplifies to the form

$$(P-P_z)\left(\frac{I_0}{A}(P-P_\phi)(P-P_y)-P^2y_0^2\right)=0 \tag{19}$$

Eq. (19) is the buckling equation for combined lateral-torsional instability of equal leg angle columns. If P_z is the smallest of the three roots of Eq. (19), the column will buckle in pure flexure about the weak axis, while in any other case the column will buckle in a combined lateral-torsional mode.

Using $E=2.6\times10^6$ psi (17.93GPa) and $G=4.25\times10^5$ psi (2.93GPa) along with the geometric characteristics of the angle sections given in Table 1, the critical buckling loads are computed for various lengths and the corresponding buckling mode is identified. The results are listed in Table 4.

5. Design guidelines

According to the design equations provided by the manufacturer (MMFG 1989), angle section columns can be treated as short or long depending on the slenderness KL/r, where L is the length, r is the radius of gyration and K is the effective length factor which depends on the boundary conditions. For simply supported ends, $K=1$.

For short columns, it is suggested that the maximum load be taken as

Table 4 Critical loads for the angle columns by simplified analysis

L (in)	4×4×¼ (lb)	4×4×⅜ (lb)	4×4×½ (lb)	6×6×¼ (lb)	6×6×⅜ (lb)	6×6×½ (lb)
24	4000	13786	33164	3029	10416	25128
30	3810	13063	31152	2766	9504	22897
36	3699	12597	29707	2622	9000	21647
42	3622	12239	28463	2535	8688	20854
48	3564	11926	25558*	2477	8476	20297
60	3469	11329	16357*	2405	8202	19526
72	3382	8779*	11359*	2363	8018	18949

*The column fails in pure flexural mode

Table 5 Maximum loads (lbs) for the angle columns according to MMFG

L (in)	4 × 4 × ¼	4 × 4 × ⅜	4 × 4 × ½	6 × 6 × ¼	6 × 6 × ⅜	6 × 6 × ½
24	13273.85*	20098.35	26472.60	13827.90*	30004.43*	50766.56
30	12092.83	17777.06	23415.10	13827.90*	30004.43*	44903.19
36	10939.02	16080.89	21181.00	13827.90*	30004.43*	40618.84
42	10049.80	14773.71	19459.23	13827.90*	28284.93	37317.01
48	9338.17	13727.58	18081.32	13827.90*	26282.07	34674.58
60	8259.65	12142.09	15992.99	13827.90*	23246.58	30669.79
72	7471.57	10983.57	14467.05	13827.90*	21028.55	27743.49

*Maximum load according to Eq. (20)

$$P=\frac{EA}{27(b/t)^{0.95}} \tag{20}$$

whereas, for long columns the maximum load is computed from

$$P=\frac{EA}{56(KL/r)^{0.55}} \tag{21}$$

The maximum load depends on the geometric characteristics as well as the longitudinal modulus E determined by tensile coupon testing. The manufacturer (MMFG) suggests to use $E = 2.6 \times 10^6$ psi (17.93GPa) and $G = 4.25 \times 10^5$ psi (2.93GPa) for the design of FRP sections. It must be stated that Eqs. (12) and (13) have been developed especially for pultruded angle columns using experimental data and curve fitting techniques. The maximum loads determined from Eqs. (12) and (13) for various lengths of the angle sections under study are listed in Table 5.

6. AISC specifications

Although the AISC Specifications (1994) applies to steel members that are characterized by plastic deformations past the yield point, it may be useful to compare the corresponding predicted loads to the experimental ones. It should be noted that FRP do not have inelastic behavior. In this case, though, we can employ as σ_y the critical stress in the uniaxial compression. The maximum longitudinal stress suggested by the manufacturer is $\sigma_y = 30{,}000$ psi (207MPa) for the angle sections under study. For single angle members subjected to compression, the maximum load is

$$P=A\ \sigma_{cr} \tag{22}$$

where, A is the cross-sectional area and σ_{cr} is the critical stress computed as follows:

$$\sigma_{cr}=Q(0.658^{Q\lambda_c^2})\sigma_y \quad \text{(ksi)} \quad \text{for} \quad \lambda_c\sqrt{Q}<1.5 \tag{23}$$

$$\sigma_{cr}=\frac{0.877}{\lambda_c^2}\sigma_y \quad \text{(ksi)} \quad \text{for} \quad \lambda_c\sqrt{Q}\geq 1.5 \tag{24}$$

and

$$\lambda_c=\frac{KL}{\pi r}\sqrt{\frac{\sigma_y}{E}} \tag{25}$$

The reduction factor Q is introduced to account for local buckling, and is computed as follows:

$$Q=1.0 \qquad \text{when} \quad \frac{b}{t}\le 0.446\sqrt{\frac{E}{\sigma_y}} \tag{26a}$$

$$Q=1.34-0.761\frac{b}{t}\sqrt{\frac{E}{\sigma_y}} \qquad \text{when} \quad 0.446\sqrt{\frac{E}{\sigma_y}}<\frac{b}{t}<0.910\sqrt{\frac{E}{\sigma_y}} \tag{26b}$$

$$Q=\frac{0.534E}{\sigma_y(b/t)^2} \qquad \text{when} \quad \frac{b}{t}>0.910\sqrt{\frac{E}{\sigma_y}} \tag{26c}$$

The maximum compressive loads determined by Eq. (22) for various lengths of the $4\times4\times¼$ angle section are listed in Table 6.

7. Simplified approach

The column approach described previously is used to compute the maximum loads and the corresponding axial stresses σ_{cr} versus the slenderness ratio KL/r_z for various values of the ratio b/t. The results are shown in Fig. 3. It is observed that for $L\ge L_{cr}$, the column buckles in a pure flexural mode about the weak z-axis, while for $L<L_{cr}$ a combined lateral-torsional mode takes place. The characteristic length L_{cr} corresponds to the transition from combined mode to pure flexural mode. The critical slenderness KL_{cr}/r_z is related to the ratio b/t as follows

$$\frac{KL_{cr}}{r_z}=6.377\left(\frac{b}{t}\right)^{1.072} \tag{27}$$

where the coefficients in Eq. (27) are determined using curve fitting techniques, see Fig. 4. It is also observed that the critical loads corresponding to the combined buckling mode are approximately

Table 6 Summary of tested and predicted loads for the $4\times4\times¼$ angle columns

L (in)	KL/r	Test (lbs)	Simplified Approach	MMFG (lbs)	AISC (lbs)	FEM (lbs)
24	30.2	7337	4000	13274	8644	5339
30	37.8	5967	3810	12093	8259	4597
36	45.3	5819	3699	10939	7813	4194
42	52.9	5789	3622	10050	7316	3949
48	60.5	5166	3564	9338	6782	3787
60	75.6	-	3469	8260	5645	3599
72	90.7	-	3382	7472	4527	3471

equal to the critical loads corresponding to pure torsional mode. Thus, it is proposed to compute the maximum load by first determining the critical slenderness using Eq. (27) for the corresponding ratio b/t, and subsequently the critical length L_{cr} and compare it with the column length L. The maximum load is then determined as

$$P_{\max}=\frac{\pi^2 EI_z}{(KL)^2} \qquad \text{for} \qquad L \geq L_{cr} \tag{28a}$$

$$P_{\max}=\frac{A}{I_0}\left(\frac{\pi^2 EC_w}{(KL)^2}+GJ\right) \qquad \text{for} \qquad L<L_{cr} \tag{28b}$$

For columns with low values of b/t, Eqs. (28) are a very good approximation to the actual critical load. For short columns, where the shear effect is predominant, the second term in Eq. (28b) with the shear modulus is important. For high values of b/t, the local effect is very weak and Eqs. (28) can be simplified to

$$P_{\max}=\frac{\pi^2 EI_z}{(KL)^2} \qquad \text{for} \qquad L \geq L_{cr},$$

$$P_{\max}=\frac{\pi^2 EI_z}{(KL_{cr})^2} \qquad \text{for} \qquad L<L_{cr} \tag{29}$$

It must be stated that the characteristic inelastic behavior for steel sections due to the presence of plastic strains does not appear in composite sections. The yield stress in composite materials coincides with the ultimate stress, thus the behavior of short members is also elastic.

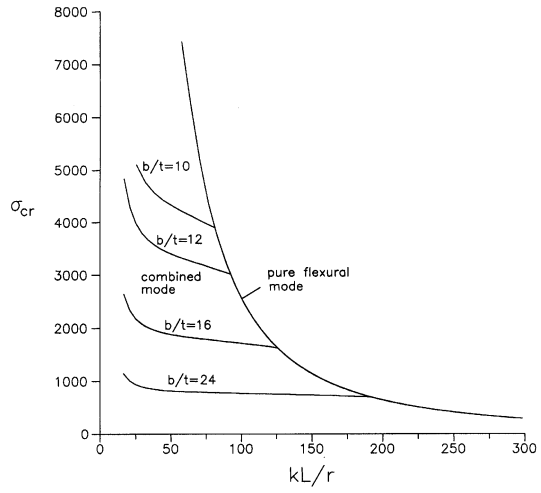

Fig. 3 Critical stress σ_{cr} vs slenderness ratio KL/r for various values of b/t

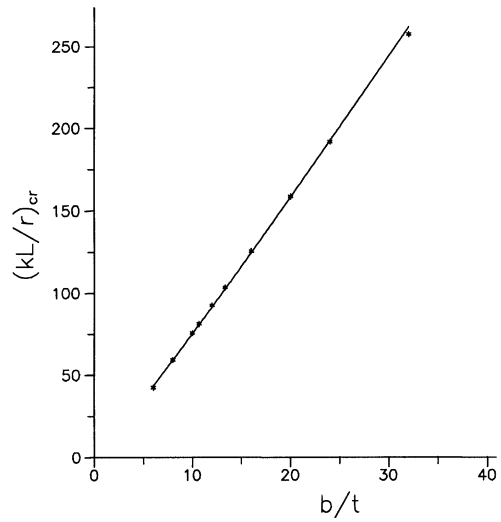

Fig. 4 Critical slenderness KL_{cr}/r versus ratio b/t

8. Experimental analysis

In this study, FRP equal-leg angle sections have been tested in compression. The specimens measured $4 \times 4 \times ¼$ inches ($10 \times 10 \times 0.65$ cm) in cross-sectional dimensions that represent the weakest shape among pultruded equal-leg angle sections. The main parameter varied in the experimental study was the length of the column. Five different lengths of 24, 30, 36, 42 and 48 inches (0.61, 0.76, 0.91, 1.07 and 1.22 m) are loaded through the centroid of the angle section, see Fig. 5(a). Each end of the specimen is placed into a steel-plate feature as shown in Fig. 5(b). Loading through the centroid is accomplished through the use of a bearing ball applied directly onto the steel loading plate. The purpose of the steel plates was to uniformly distribute the load and maintain the angle configuration at the extremities of the section. The rounded loading point allowed the section to rotate freely, thereby modeling a pin-ended structure.

During testing, the rate of load application was approximately 30 lb/sec (133.5 N/sec). An electronic device for measuring the axial deformation of the angle section was used. The specimens were loaded to the point of failure, defined here as the point where large deformations occurred accompanied by a decrease in the load carrying capacity of the angle sections. All specimens tested failed by lateral-torsional buckling. No signs of failure at the ends of the specimens, such as cracking or crushing of the resin and fibers, appeared during tests. Fig. 4 shows the load-deflection curves for each specimen, while the corresponding critical loads are listed in Table 7. The point where buckling was initiated corresponds to the critical buckling load. Buckling does not lead to collapse of the column. The lateral-torsional mode observed in the specimens tested corresponds to a stable post-buckling behavior (mild buckling). However, further load increase past the critical state is associated with large deformations. Thus, the column retains a postbuckling strength that is almost 10% of the critical buckling load. Fig. 7 shows the buckled shape of a 42 in (1.07m) long angle specimen.

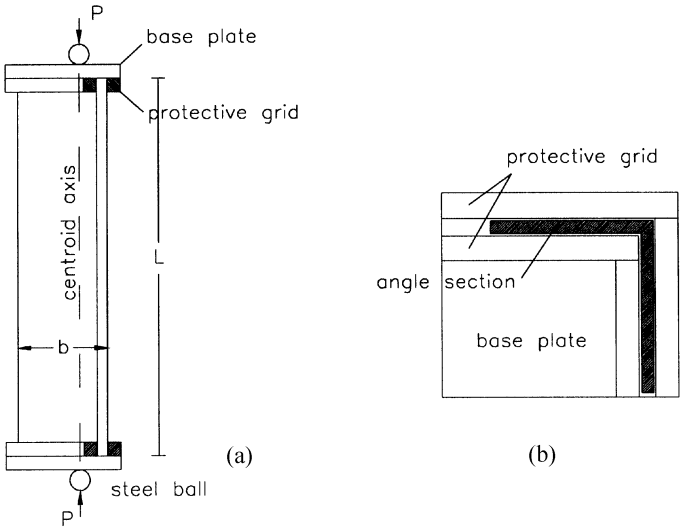

Fig. 5 (a) Experimental setup, (b) Base plate and protective grid

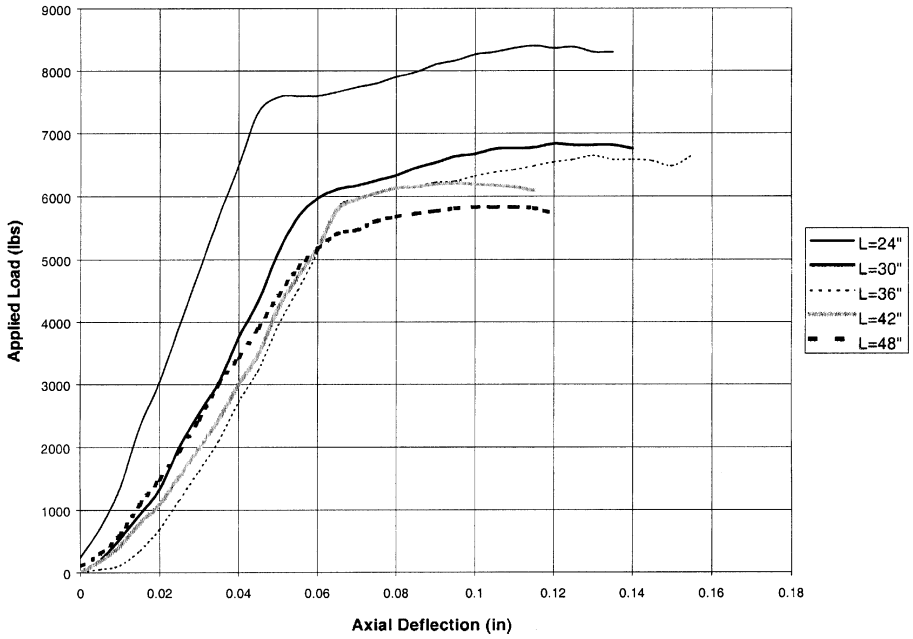

Fig. 6 Experimental curves: compression load vs axial displacement

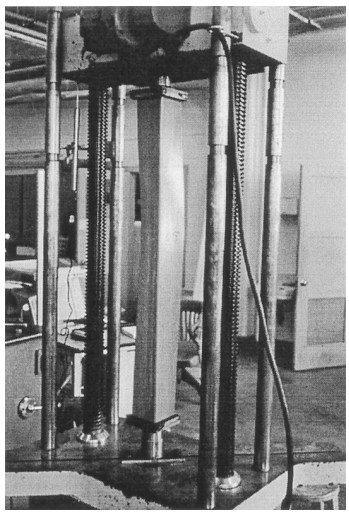

Fig. 7 Buckled shape of a 42 in long specimen under compression

9. Interpretation of the results and discussion

The analytical results obtained by the simplified approach and the MMFG and AISC design guidelines as well as the numerical and experimental results for the $4 \times 4 \times \frac{1}{4}$ angle section are presented in Table 6. Fig. 8 shows the maximum loads versus the slenderness ratio KL/r for both the predicted and the experimental results. It is clear that the maximum loads predicted according to

Table 7 Load-deflection data for the tested 4 × 4 × ¼ FRP angle columns

Deflection (in)	L=24 (in)	L=30 (in)	L=36 (in)	L=42 (in)	L=48 (in)
0.000	241.2	0.0	10.1	0.0	100.5
0.005	712.0	201.0	50.3	180.9	301.5
0.010	1346.7	542.7	110.5	422.1	603.0
0.015	2311.5	924.6	351.8	783.9	1085.4
0.020	3035.1	1326.6	693.5	1085.4	1487.4
0.025	3939.6	1989.9	1155.8	1527.6	1929.6
0.030	4824.0	2532.6	1618.1	1969.8	2432.1
0.035	5688.3	3035.9	2100.5	2432.1	3015.0
0.040	6492.3	3758.7	2723.6	2994.9	3437.1
0.045	7336.5	4341.6	3226.1	3477.3	3899.4
0.050	7577.8	5105.4	3949.7	4221.0	4422.0
0.055	7597.6	5668.2	4512.5	4723.5	4864.2
0.060	7597.6	5967.0	5115.5	5185.8	5165.7
0.065	7660.0	6110.4	5819.0	5788.8	5406.9
0.070	7738.1	6170.7	5959.7	5949.6	5467.2
0.075	7798.8	6251.1	6040.1	6050.1	5607.9
0.080	7899.3	6331.5	6140.6	6130.5	5678.0
0.085	7979.7	6452.1	6160.7	6150.5	5728.5
0.090	8100.3	6532.5	6221.0	6190.5	5768.5
0.095	8160.6	6633.0	6241.1	6210.9	5808.9
0.100	8261.1	6673.2	6321.5	6190.8	5829.9
0.105	8301.3	6753.2	6381.6	6170.9	5829.9
0.110	8361.6	6763.2	6422.0	6150.6	5829.9
0.115	8401.8	6773.7	6482.3	6090.3	5808.9
0.120	8361.6	6834.0	6542.6	-	5728.5
0.125	8381.7	6813.9	6582.8	-	-
0.130	8301.3	6813.9	6643.1	-	-
0.135	8301.3	6813.9	6582.8	-	-
0.140	-	6757.3	6582.8	-	-
0.145	-	-	6562.7	-	-
0.150	-	-	6482.3	-	-
0.155	-	-	6642.1	-	-

the manufacturer's guidelines are not reliable, compared to other analytical and experimental results. The experimental results do not correlate well with the AISC predictions. In fact, AISC guidelines predict 30% to 50% higher loads compared to the experimental ones. AISC methodology for design of angle columns is not valid for composite members because the longitudinal modulus for composite materials is at least ten times less than the steel modulus. Also, the effect of residual stresses built into the AISC expressions is not the same as in the composite angles. Thus, the slenderness required for pure flexural buckling is smaller than the one corresponding to an identical composite member. This effect is shown in Fig. 3, where the critical stress σ_{cr} is plotted versus the

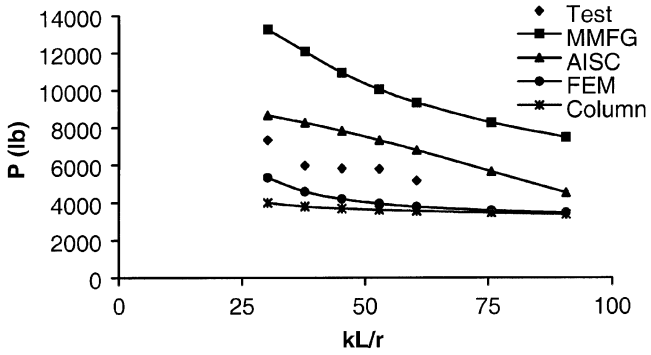

Fig. 8 Predicted and experimental maximum loads vs slenderness ratio KL/r

member slenderness KL/r for various cases of b/t. It is observed that transition from combined lateral-torsional to pure flexural mode occurs for KL_{cr}/r, where the critical slenderness can be related to b/t. Furthermore, the shear modulus G for composite materials takes low values and the combined buckling load is significantly affected for small values of b/t.

The critical mode predicted by the finite element method for all models was lateral-torsional buckling, that is in full agreement with the experimentally observed failure mode. The finite element results and the simplified approach values are in good correlation with each other. For the sections under study, both methods resulted in conservative values. Thus, the simplified approach can safely be adopted for the design of pultruded angle columns.

10. Conclusions

An experimental study is used herein to validate the predicted maximum loads for equal leg angle section composite members subjected to axial compression. Prediction of the buckling load and the corresponding mode is very important for the determination of the axial strength of pultruded members because instability failure leads to collapse of the whole member. The finite element method has been employed to predict the buckling loads as well as the buckling mode failure for commercially available pultruded angle sections. The analytical methods presented here are based on the description of the cross-section used by the manufacturer. Thin-walled angle sections used as compression members fail primarily due to lateral-torsional buckling, while if the legs are relatively thick, flexural buckling is the critical mode. A simplified approach is proposed for determining the maximum compressive load of angle sections. Comparison between experimental and analytical results shows that the proposed simplified approach can be efficiently used for the design of pultruded angle sections.

References

American Institute of Steel Construction (AISC) (1994), *Manual of Steel Construction -LRFD*, 2nd ed., Chicago, IL.

Barbero, E.J. and Raftoyiannis, I.G. (1993), "Euler buckling of pultruded composite columns", *Composite*

Structures, **24**, 139-147.
Barbero, E.J., Godoy, L.A. and Raftoyiannis, I.G. (1996), "Finite elements for three-mode interaction in buckling analysis", *Int. J. Num. Method in Eng.*, **39**, 469-488.
Brush, D.O. and Almroth, B.O. (1975), *Buckling of Bars, Plates and Shells*, McGraw-Hill, NY.
Eterovic, A.L., Godoy, L.A. and Prato, C.A. (1990), "Initial postcritical behavior of thin-walled angle section columns", *ASCE, J. Engng. Mech.*, **116**(11), 2573-77.
Gibson, R.F. (1994), *Principles of Composite Material Mechanics*, McGraw-Hill, NY.
Morrison Molded Fiber Glass Co. (1989), *Extren Design Manual*, Bristol, VA, USA.
Raftoyiannis, I.G. (1994), "Buckling mode interaction in FRP columns", Ph.D. Dissertation, West Virginia University, WV.

Notation

A	cross-sectional area
A_{ij}	membrane stiffness coefficients
B_{ij}	membrane-flexural coupling stiffness coefficients
C_w	warping constant
$\{\delta\}$	nodal displacement vector
D_{ij}	flexural stiffness coefficients
ε_i	strains
E	longitudinal modulus of elasticity
$\{f\}$	nodal force vector
ϕ	angle of twist
G	shear modulus
I	moment of inertia
J	torsion constant
$\overline{Q}_{ij}$	transformed layer stiffness
κ_i	curvatures
$[K]$	stiffness matrix
$[K_\sigma]$	load-geometry matrix
λ	load factor
L	column length
$\{M\}$	moment resultant vector
$\{N\}$	stress resultant vector
P	applied load
σ_i	stresses
S_i	out-of-plane shear resultants
t	thickness
U	total potential energy
v	lateral deflection along y-direction
w	lateral deflection along z-direction